



A three-part bias correction of simulated European river runoff to force ocean models

Stefan Hagemann*, Thao T. Nguyen and Ha T. M. Ho-Hagemann

Institute of Coastal Systems – Analysis and Modelling, Helmholtz-Zentrum Hereon, Max-Planck-Str. 1, 21502 Geesthacht, Germany

* Correspondence: Dr. Stefan Hagemann, stefan.hagemann@hereon.de

1 Abstract

2 In ocean or Earth system model applications, the riverine freshwater inflow is an important flux
3 affecting salinity and marine stratification in coastal areas. However, in climate change studies,
4 the river runoff based on climate model output often has large biases on local, regional or even
5 basin-wide scales. If these biases are too large, the ocean model forced by the runoff will drift
6 into a different climate state compared to the observed state, which is particularly relevant for
7 semi-enclosed seas such as the Baltic Sea. In order to meet the requirements for low biases in
8 river runoff, we have developed a three-part bias correction that includes different correction
9 factors for low, medium and high percentile ranges of river runoff over Europe. Here, we
10 present an experimental setup using the Hydrological Discharge (HD) model and its high-
11 resolution (1/12°) grid. First, bias correction factors are derived at the locations of the
12 downstream stations with available daily discharge observations for many European rivers.
13 These factors are then transferred to the respective river mouths and mapped to neighbouring
14 grid boxes belonging to ungauged catchments. The results show that the bias correction
15 generally leads to an improved representation of river runoff. Especially over Northern Europe,
16 where many rivers are regulated, the three-part bias correction provides an advantage compared
17 to a bias correction that only corrects the mean bias of the river runoff. Evaluating two NEMO
18 ocean model simulations in the German Bight indicated that the use of the bias corrected
19 discharges as forcing leads to an improved simulation of sea surface salinity in coastal areas.
20 Although in the present study, the bias correction is tailored to the high-resolution HD model
21 grid over Europe, the methodology is suitable for any high-resolution model region with a
22 sufficiently high coverage of river runoff observations. It is also noted that the methodology is
23 applicable to river runoff based on climate hindcasts as well as on historical climate simulations
24 where the sequence of weather events does not match the actual observed history. Therefore, it
25 may also be applied in climate change simulations.

26 **Keywords:** Bias correction, river runoff, discharge, high resolution, Europe

27

28 1 Introduction

29 River runoff (or discharge/streamflow) is an important component of the global hydrological
30 cycle, accounting for about one-third of precipitation over land areas. It closes the water cycle
31 between land and ocean and influences various ocean properties, in particular the salinity of
32 coastal and semi-enclosed seas (e.g. Väli et al., 2013), the ocean stratification in shelf areas
33 (e.g. Hordoir and Meier, 2010) such as the German Bight (Becker et al., 1992), and the



34 thermohaline circulation in different regions (e.g. Hordoir et al., 2008; Lehmann and
35 Hinrichsen, 2000; Marzeion et al., 2007). In addition, river runoff and associated nutrient loads
36 are important factors influencing marine ecosystem functioning (Daewel and Schrum, 2017).

37 Consequently, river runoff needs to be adequately represented in studies of the impacts of
38 climate change on the marine environment or in coupled Earth system studies. In such studies,
39 the atmospheric data used to force the respective ocean model are usually taken from climate
40 models, reanalysis products or hydrological models. Here, it is desirable that the river runoff is
41 consistent with the atmospheric forcing. In previous modelling studies, runoff was often taken
42 from climatology or discharge observations, especially when hindcasts were used. However,
43 this is not a recommended approach for climate change studies where consistently simulated
44 river runoff should be used. Runoff from the driving climate, land surface or hydrological model
45 will contain biases, e.g., due to biases in precipitation and/or uncertainties in the land surface
46 representation of the model. Many simulations of historical daily river runoff show common
47 biases in the tails of their distributions, with high discharges underestimated and low discharges
48 overestimated (Farmer et al., 2018, and references therein). If the basin-wide biases are too
49 large, a bias correction of the simulated discharge would be necessary to avoid the ocean model
50 drifting into a different climate state compared to the observed state. This is particularly relevant
51 for semi-enclosed seas such as the Baltic Sea. For example, for Baltic Sea ocean models, the
52 mean long-term bias of river runoff must be less than 7% (Hagemann and Stacke, 2022).

53 The bias correction of river runoff is an approach that has been used particularly for short-
54 term hydrological forecasts and ensemble predictions of up to six months. Here, Kim et al.
55 (2021) provide examples of related studies. Recently, bias correction of river runoff has also
56 been applied in the context of climate change. Quantile mapping based approaches are often
57 used for such bias correction, as this usually leads to a large improvement in the representation
58 of discharge of the considered river. For example, Budhathoki et al. (2022) used quantile
59 mapping to correct discharge bias in the Chao Phraya River basin (Thailand), and Daraio (2020)
60 used it for two basins in New Jersey (USA). However, Madadgar et al. (2014) noted that
61 quantile mapping was not always successful in improving the initial forecast trajectory. In their
62 application for the Sprague River (southern Oregon, USA), the skill of the forecast actually
63 deteriorated when the quantile mapping technique was used. Similarly, Malek et al. (2022) used
64 a quantile mapping based bias correction of discharge and showed that ex-post corrections of
65 simulated discharge do not necessarily reduce biases in the simulation of key processes and in
66 some cases can severely degrade system simulations.

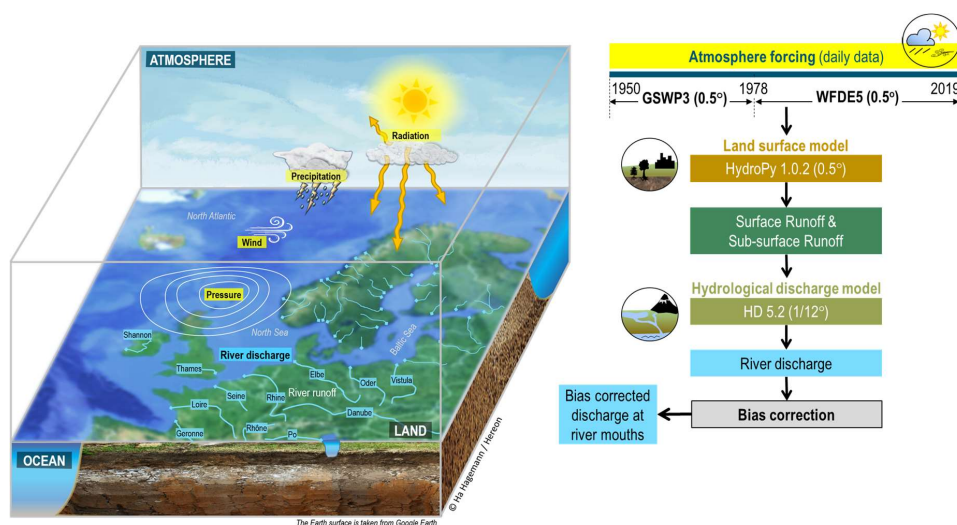
67 Consequently, the aim of the present study was to develop a bias correction method sufficient
68 to meet the requirements of ocean models in large-scale climate change studies. Note that we
69 did not aim for the most accurate reproduction of observed discharge characteristics, as required
70 for short-term hydrological predictions and flood forecasts used by water resource decision
71 makers (e.g. Shi et al., 2008). In order to maintain a high degree of consistency of simulated
72 runoff with the meteorological patterns in the driving (on- or offline) climate model (or data),
73 a bias correction with as little modification of the daily runoff curves as possible is desired.
74 Thus, our target is a simple bias correction that corrects the mean bias and the tail biases of the
75 discharge distribution in climate change applications of ocean or coupled system models. The
76 bias correction factors should be transferable from downstream stations to river mouths as well
77 as to neighbouring ungauged catchments. Furthermore, it should be applicable to climate model
78 or Earth system model data that lack the observed sequence of actual discharge events.



79 The manuscript is organised as follows. Section 2 describes how the simulated discharges
 80 were generated and the newly developed bias correction methodology, as well as the data,
 81 models and metrics used in this study. Sections 3 and 4 evaluate the simulated and bias corrected
 82 discharges and present the effects of the bias correction for station locations and sea basin
 83 inflows, respectively. Finally, Section 5 concludes with a summary and conclusions.

84 2 Data and Methods

85 To generate the freshwater inflow from rivers to the ocean, we used an experimental setup
 86 analogous to Hagemann and Stacke (2022). Here we used two atmospheric forcing datasets
 87 (Sect. 2.1) and the same model chain of two large-scale hydrological models. The global
 88 hydrological model HydroPy (Sect. 2.2) was used to generate the input to the Hydrological
 89 Discharge (HD) model (Sect. 2.3) at the resolution of the atmospheric forcing data (0.5°). These
 90 input data of surface and sub-surface runoff were then interpolated onto the HD model grid and
 91 the HD model was used to simulate daily discharges from land to sea. Subsequently, we bias
 92 corrected these time series as described in Section 2.4 to generate bias corrected discharges at
 93 coastal ocean boxes of the European HD model domain from 1901-2019. Note that we
 94 combined the simulations based on two different atmospheric forcing datasets to cover the
 95 whole 20th century and to include the more recent years in the bias corrected discharge time
 96 series. Such an approach was also used in the second phase (ISIMIP, 2023) of the Inter-Sectoral
 97 Impact Model Inter-Comparison Project (ISIMIP; Warszawski et al., 2014). Figure 1
 98 summarises the experimental setup. Section 2.5 refers to the observational data that are used in
 99 the evaluation of the model results. Finally, the evaluation metrics used in the analysis of the
 100 results are presented in Sect. 2.7.



101

102

103 **Figure 1.** Overview on the main steps of generating bias corrected river discharge at HD
 104 river mouths.

105



106 **2.1 Atmospheric forcing**

107 We used two atmospheric datasets specifically generated for forcing global hydrological
108 models.

109 The Global Soil Wetness Project Phase 3 (GSWP3; Dirmeyer et al., 2006; Kim, 2017)
110 dataset is available at 0.5° resolution from 1901-2014. To generate the GSWP3 dataset, the 20th
111 Century Reanalysis (20CR; Compo et al., 2011) was first dynamically downscaled onto the
112 T248 (~0.5°) grid using a spectral nudging technique (Yoshimura and Kanamitsu, 2008) in a
113 Global Spectral Model (GSM). Observation-based bias correction procedures were then applied
114 to the downscaled data to obtain daily time series.

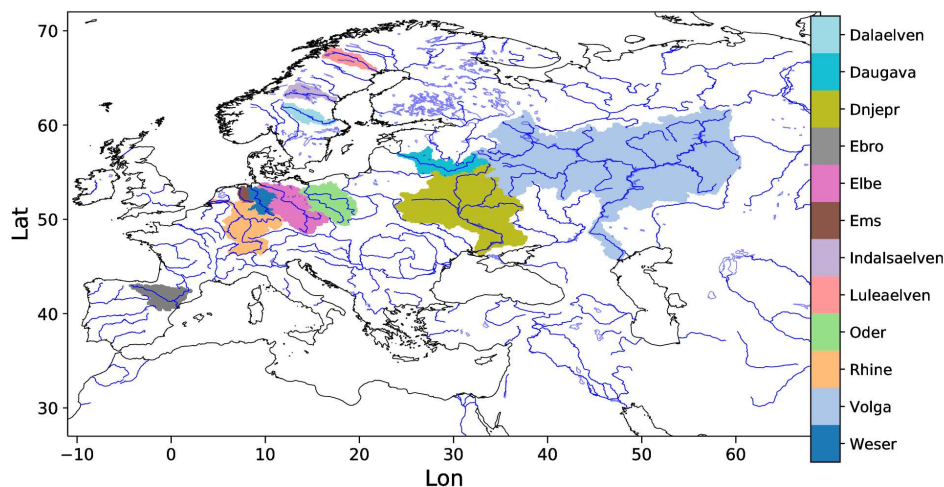
115 To generate the WFDE5 dataset (Cucchi et al., 2020), the WATCH Forcing Data (WFD)
116 methodology (Weedon et al., 2011) was applied to surface meteorological variables from the
117 ERA5 reanalysis (Hersbach et al., 2020) to obtain bias corrected time series. ERA5 is the fifth
118 generation of atmospheric reanalysis produced by the European Centre for Medium-Range
119 Weather Forecasts (ECMWF). WFDE5 is provided at 0.5 spatial resolution from 1979-2019.

120 **2.2 HydroPy setup**

121 HydroPy (Stacke and Hagemann, 2021) was driven by daily forcing data from 1901-2019.
122 Daily input fields of surface and subsurface runoff were generated at a resolution of 0.5°.
123 Analogous to the ERA5 forced simulation in Hagemann and Stacke (2022), precipitation, 2m
124 temperature, downwelling shortwave and longwave radiation, 2m specific humidity, surface
125 pressure and 10m wind are used as forcing from the respective forcing dataset. We performed
126 a spin-up simulation over 50 iterations of the year 1901 with the GSWP3 forcing (cf. Stacke
127 and Hagemann, 2021) to initialize the storages in the HydroPy model and to avoid any drift
128 during the actual simulation period. We then forced HydroPy with the GSWP3 data from 1901-
129 1978 and continued with the WFDE5 data from 1979-2019. We also conducted a GSWP3
130 forced simulation from 1979-2014 in order to derive bias correction parameters for the earlier
131 period. For our analysis, we focus on the years from 1950 onwards so that we have an additional
132 transient spin-up of 49 years.

133 **2.3 HD model setup**

134 To simulate discharge, the HD model (Hagemann et al., 2020) used the daily input fields of
135 surface and subsurface runoff that were generated by HydroPy from the GSWP3 and WFDE5
136 data (see Sect. 2.2). As the time step of these runoff data is one day, the time step of the HD
137 model was also set to one day. However, an internal time step of 0.5 hours is used for the flow
138 within the river, as the minimum travel time through a grid box is limited by the chosen time
139 step. The HD model v5.2.0 (Hagemann et al., 2023a) was applied over the European domain,
140 which covers the land areas between -11°W to 69°E and 27°N to 72°N. The domain, along with
141 a number of rivers specifically noted in this study, is shown in Figure 2. In the following, we
142 refer to the WFDE5-based discharges as HD5-WFDE5 and to the GSWP3-based discharges as
143 HD5-GSWP3.



144

145 **Figure 2.** European HD model domain and catchment areas for selected rivers

146 **2.4 Bias correction of river runoff**

147 We have developed a three-part bias correction method for river runoff with different correction
 148 factors for low, medium and high percentiles. These are first calculated at the station locations
 149 and then applied to the respective river mouths. Finally, an interpolation is performed to
 150 neighbouring coastal mouth points for which no downstream observations are available in the
 151 respective catchment. This procedure is summarised in Figure 3. The three percentile ranges
 152 for daily discharge q_i are classified by

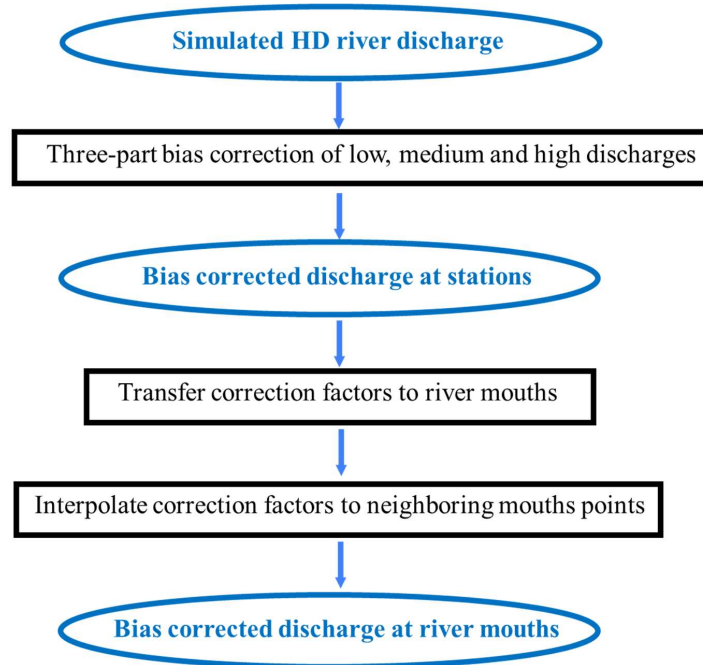
- 153
- Low (L): $q_i \leq Q_p$
 - 154 • Medium (M): $Q_p < q_i < Q_{100-p}$
 - 155 • High (H): $q_i \geq Q_{100-p}$

156 Here, Q_p denotes the p^{th} percentile of the daily discharge and p was set to 20. The percentiles
 157 Q_p and Q_{100-p} were determined separately for the observed and the simulated discharges at the
 158 downstream station locations and then the mean discharges \bar{q}_R were calculated for the three
 159 percentile ranges $R \in \{L, M, H\}$. Note that for these calculations only those days were
 160 considered for which an observed discharge was available. Then, the mean bias b_R (in %) was
 161 calculated for each percentile range and a correction factor f_R to remove the bias was derived as

162

$$f_R = \frac{100}{b_R + 100}$$

163



164

165 **Figure 3.** Steps to derive bias corrected discharge at river mouths from simulated
166 discharges.

167 For the evaluation of the bias correction in Sect. 3, these correction factors were applied to
168 the simulated discharges at the station locations. As the correction factors are independent of
169 the absolute amount of discharge, they could be applied to the respective river mouths. For each
170 river mouth with more than one inflow ($j > 1$) for which a correction factor $f_{R,j}$ is determined, a
171 combined correction factor is obtained by calculating an average weighted by the respective
172 mean inflows Q_j .

173

$$\bar{f}_R = \frac{\sum_j f_{R,j} * Q_j}{\sum_j Q_j}$$

174 From these river mouths, an interpolation is performed to neighbouring coastal mouth points
175 for which no downstream observations are available in the respective catchment. This
176 interpolation was motivated by the fact that the general pattern of bias of neighbouring rivers
177 is often similar (cf. Sect. 3.1). The interpolation is performed by inverse distance weighting
178 from the four closest (or fewer) river mouths within a search radius of 200 km. If no river mouth
179 with a correction factor was found within the search radius, the correction factor was set to one
180 (i.e. no correction).

181 Note that the bias correction can lead to spurious daily jumps in discharge when the
182 percentile boundary is crossed and the bias correction factors differ between the percentile
183 ranges. In order to reduce this effect, a smoothing radius of $\Delta s = 0.05$ was introduced around
184 the percentile boundaries, which was applied at both station locations and river mouths.



185 For $(1 - \Delta s) * q_p < q_i < (1 + \Delta s) * q_p$:

186
$$\tilde{q}_i = q_i * (f_L + (f_M - f_L) * \frac{(q_i - (1 - \Delta s) * q_p)}{2 * \Delta s * q_p})$$

187 For $(1 - \Delta s) * q_{100-p} < q_i < (1 + \Delta s) * q_{100-p}$:

188
$$\tilde{q}_i = q_i * (f_M + (f_H - f_M) * \frac{(q_i - (1 - \Delta s) * q_{100-p})}{2 * \Delta s * q_{100-p}})$$

189 The bias correction procedure corrects the days that fall into the different percentile ranges.
190 However, this does not necessarily mean that it also corrects the whole distribution into the
191 three percentile ranges. Particularly, if the biases in these ranges are quite different, the days
192 may change their class and order within the distribution.

193 In order to apply the three-part bias correction to the simulated discharge time series from
194 1901-2019, two sets of bias correction factors were derived. The first set uses HD5-WFDE5
195 and discharge station observations for the period 1979-2014. This set was used to bias correct
196 the simulated discharge at HD river mouths from 1979-2019. The second set uses a further
197 discharge simulation where we continued HD5-GSWP3 utilizing the GSWP3 forcing up to
198 2014. Again, the set of bias correction factors was derived for the period 1979-2014 using
199 discharge station observations. This set was then used to bias correct the simulated discharge at
200 the HD river mouths from 1901-1978.

201 **2.5 Observed discharge data**

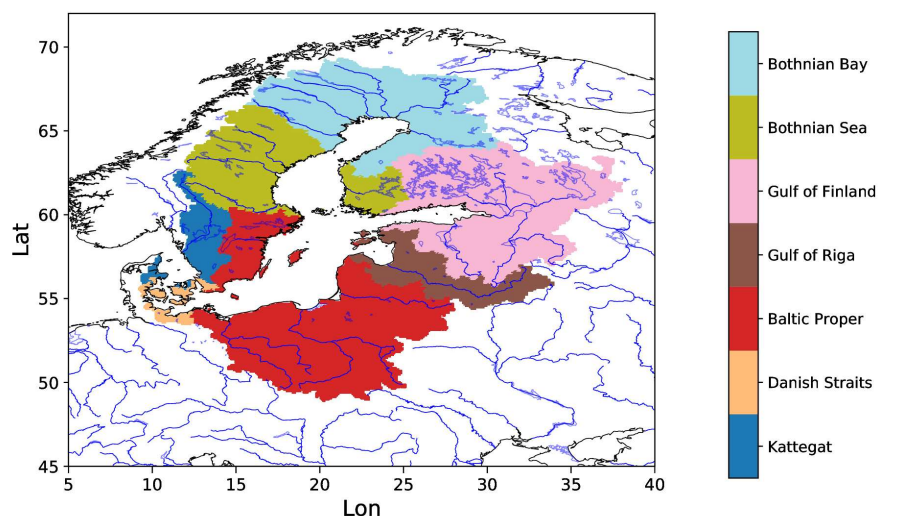
202 We used available daily discharge data from downstream gauges for many rivers across Europe
203 with a catchment area of about 1000 km² or more. These station data were obtained from Global
204 Runoff Data Centre (GRDC) and various agencies and institutions listed in table 2 of Hagemann
205 and Stacke (2022). In addition, French discharge data were accessed from the E.U. Copernicus
206 Marine Service Information. In order to allow an assessment of the discharge at the river
207 mouths, we considered basin-wide estimates from three different sources.

208 For the Baltic Marine Environment Protection Commission – also known as the Helsinki
209 Commission (HELCOM), Svendsen and Gustafsson (2022) provided annual waterborne
210 inflows into the seven main sub-basins of the Baltic Sea (Figure 4 – upper panel) from 1995 to
211 2020. Waterborne inflows comprise the sum of river runoff and direct inflows, i.e. flows from
212 point sources discharging directly into the Baltic Sea. These point sources are not included in
213 our experimental setup or in the bias correction. However, their contribution to the total
214 waterborne inflow to the Baltic Sea is only about 1% (HELCOM, 1998).

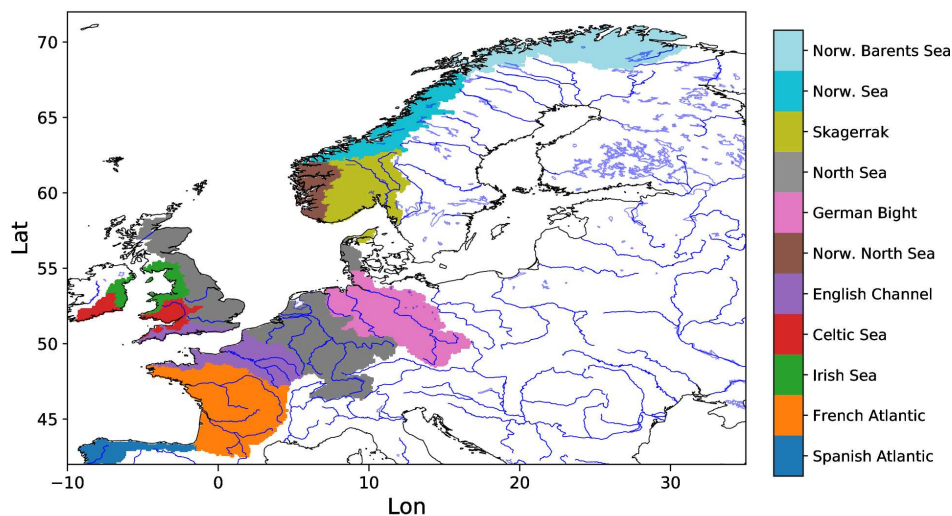
215 Under the umbrella of the OSPAR Convention (Convention for the Protection of the Marine
216 Environment of the North-East Atlantic), the IGC-EMO (Intersessional Correspondence Group
217 for Eutrophication Modelling) database (Lenhart et al., 2010) of daily riverine freshwater
218 inflows and nutrient loads was compiled by Van Leeuwen and Lenhart (2021), covering the
219 major rivers discharging into the Baltic Sea, the North Sea and the Northeast Atlantic. An
220 updated database covering a total of 370 rivers was mapped onto the flow grid of the European
221 1/12° domain of the HD model by Van Leeuwen and Hagemann (2023). The associated
222 catchment areas of these rivers, which flow into a particular specific sea basin, do not cover the



223 entire catchment area of the respective basin (see Table 1) so that the total inflow of the sea
224 basin is underrepresented by the IGC-EMO data. To generate basin-wide estimates, we have
225 up-scaled these values by dividing the integrated IGC-EMO river discharges in a basin by the
226 fractional coverage of the entire basin catchment on the HD grid. Basin estimates for which the
227 fractional coverage is less than 75% are considered to be highly uncertain and are therefore
228 provided for completeness only, but are not included in the assessment of simulated inflows.



229



230

231 **Figure 4.** Selected HELCOM (upper panel) and OSPAR (lower panel) basins for which
232 inflows are considered. For OSPAR, the Spanish Atlantic basin is limited to the coast
233 of Northern Spain.

234



235
236

Table 1. Sea basin catchment areas on the HD model grid and the fractional catchment coverage of the associated IGC-EMO rivers.

Sea basin	HD Area [km ²]		Coverage
	IGC-EMO	Total	
Baltic Sea	1513967	1671823	90.6%
Bothnian Bay	238898	258420	92.4%
Bothnian Sea	199908	219375	91.1%
Gulf of Finland	379628	412412	92.1%
Gulf of Riga	124386	134025	92.8%
Baltic Proper	494929	551295	89.8%
Danish Straits	6731	19417	34.7%
Kattegat	69487	76876	90.4%
Norwegian Barents Sea	0	81004	0.0%
Norwegian Sea	0	58408	0.0%
Skagerrak	89060	101787	87.5%
North Sea	514334	599755	85.8%
German Bight	201233	208807	96.4%
Norwegian North Sea	4590	31327	14.7%
English Channel	94327	122235	77.2%
Celtic Sea	41122	44845	91.7%
Irish Sea	29748	35584	83.6%
French Atlantic	207657	257981	80.5%
Northern Spanish Atlantic	17692	46574	38.0%

237

238 In addition, we used estimates of long-term mean sub-basin-wide inflows to the North Sea
 239 and Northeast Atlantic, published directly by OSPAR (Farkas and Skarbøvik, 2021). Figure 4
 240 (lower panel) shows the selected OSPAR basins for which the inflows are considered. It should
 241 be noted that the sea basin inflows provided by the different OSPAR countries are not
 242 consistent. Some countries include discharge estimates for unmonitored areas, while others do
 243 not (Table 2). In addition, the sea basin catchment coverage of the monitored areas varies
 244 between the countries. Note also that we have excluded the Spanish Atlantic from our
 245 comparisons for the following reason. Here, we limited the Spanish Atlantic basin to the coast
 246 of northern Spain (see Figure 4 – lower panel) to allow a comparison with the IGC-EMO data
 247 as the IGC-EMO data only cover rivers in this region, hereafter referred to as NSpA. These
 248 rivers cover about 38% of the total NSpA area on the HD model grid (Table 1), while the
 249 OSPAR data for NSpA cover about 50% (23201 km²; Farkas and Skarbøvik, 2021). However,
 250 the associated IGC-EMO discharge from 1961-1990 (629 m³/s) is 75 % larger than the OSPAR
 251 long-term mean average (359 m³/s). Therefore, both inflow values are unlikely to be
 252 representative for the NSpA region and this region is not considered in the following.

253

254



255 **Table 2.** Country catchment coverage of OSPAR data and inclusion of estimates for
 256 unmonitored areas (Borgvang et al., 2008). NI means that no information on the
 257 coverage was provided.

Country	Coverage	Unmonitored
Belgium	> 90%	No
Denmark	NI	Yes ³
France	84%	Yes
Germany	>90%	No ¹
Ireland	NI	Yes
Netherlands	>90%	No
Norway	ca. 50%	Yes
Portugal	NI	No
Spain	NI	No
Sweden	88.7%	Yes
United Kingdom	ca. 80% ²	No

258
 259
 260

¹ Only for Eider river
² 10% in direct discharge
³ e.g. Farkas and Skarbovik (2021)

261 2.6 Ocean model experiments

262 To assess the effect of using bias corrected river discharge on simulated salinity in the German
 263 Bight, we used version 3.6 of the Nucleus for European Modelling of the Ocean (NEMO;
 264 Madec et al., 2017) and adopted a domain setup used by Ho-Hagemann et al. (2020). This
 265 domain covers the region of the north-west European shelf, the North Sea and the Baltic Sea
 266 between 19.89 E to 30.16 E and 40.07 N to 65.93 N with a resolution of two nautical miles (ca
 267 3.6 km). We used the atmospheric forcing from ERA5 and the ocean boundary forcing from
 268 the ECMWF Ocean Reanalysis System 5 (ORAS5; Zuo et al., 2019) to conduct two simulations
 269 from 2010 to 2018. In these two simulations, the daily riverine inflow into the ocean was taken
 270 from the uncorrected and bias corrected discharges of HD5-WFDE5, which were converted to
 271 the NEMO grid using a procedure of Nguyen et al. (2024). For each HD model river mouth
 272 box, we associated the nearest coastal ocean box on the NEMO grid if such a box was found
 273 within a search radius of 200 km. Such a large radius is necessary because the NEMO coastline
 274 is very smooth, so many estuaries and bays in the HD model grid are not resolved by NEMO.
 275 If no ocean box was found, the corresponding HD model box was not linked. Consequently,
 276 the simulated discharge data at the river mouths were placed as freshwater inflow into the
 277 corresponding NEMO grid boxes.

278 2.7 Evaluation metrics

279 The evaluation of the simulated discharge was performed for the grid boxes corresponding to
 280 the discharge station locations within the river network. For the evaluation at these station
 281 locations, we used the mean bias and the Kling-Gupta efficiency (KGE; Gupta et al., 2009;
 282 Kling et al., 2012). Both metrics were calculated with simulated and observed daily discharge
 283 time series for the period considered, using only those days for which observed data are
 284 available. The KGE is a quality metric combining bias, correlation and coefficient of variation.
 285 If a simulated discharge time series has a KGE > -0.41, then it is a better representation of the
 286 observations than the use of the observed long-term mean discharge (Knoben et al., 2019). Note
 287 that many ocean model applications still use the latter method.

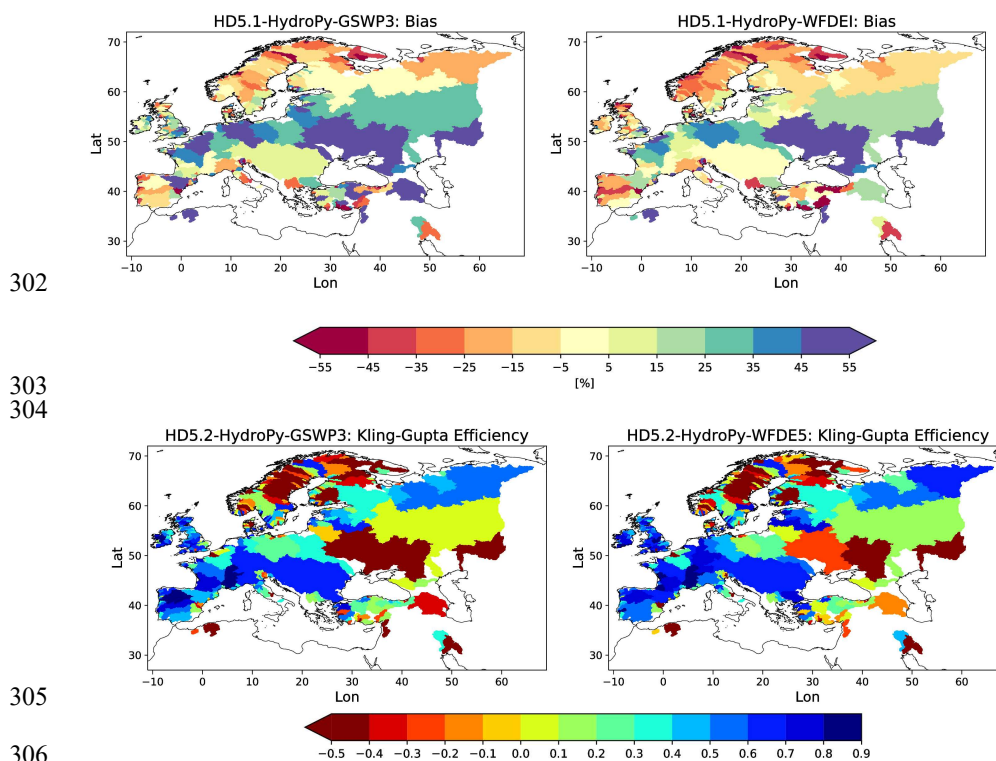


288 **3 Evaluation of the bias correction**

289 Below, various metrics have been calculated at the station locations and at the river mouths.
 290 However, these measures have been assigned to the respective catchment areas for the purpose
 291 of graphical presentation.

292 **3.1 Evaluation of simulated discharge**

293 The distribution of bias and KGE for HD5-GSWP3 and HD5-WFDE5 during 1979-2014
 294 (Figure 5) is quite similar to the pattern shown by Hagemann and Stacke (2022) for the ERA5-
 295 based discharge. For both simulations, the general discharge behaviour is well captured (KGE
 296 > 0.4) for many European rivers, especially in Northern Iberia, Western and Central Europe,
 297 and over Northern Russia (Figure 5, lower row). As expected (cf. Hagemann et al., 2020), larger
 298 deviations of the simulated from observed discharges occur for rivers that are heavily
 299 influenced by human activities such as water abstraction, e.g. for irrigation, and regulation, e.g.
 300 by dams. This is the case for many Scandinavian and Turkish rivers as well as the Volga and
 301 Don.



302
 303
 304 **Figure 5.** Mean discharge bias [%] (upper row) and Kling Gupta efficiencies (lower row)
 305 for HD5-GSWP3 (left) and HD5-WFDE5 (right) during 1979-2014.

310 In general, the HD5-WFDE5 discharges are slightly drier than the HD5-GSWP3 discharges,
 311 as indicated by larger dry biases in Northern Europe and smaller wet biases in Central Europe.



312 Despite the differences in bias distribution, the KGEs of HD5-WFDE5 are similar to or slightly
 313 better than those of HD5-GSWP3. Compared to the ERA5-based discharge of Hagemann and
 314 Stacke (2022), HD5-WFDE5 tends to have smaller discharge biases and better KGEs. This is
 315 an expected behaviour caused by the application of a bias correction methodology to the ERA5
 316 data in the generation of the WFDE5 data (cf. Sect. 2.1). An exception to this general
 317 improvement occurs over Northern Europe, where the dry bias of HD5-WFDE5 tends to be
 318 slightly larger and the KGEs lower. Note that Hagemann and Stacke (2022) attributed the dry
 319 bias over Northern Europe to an overestimation of the evapotranspiration simulated by
 320 HydroPy.

321 3.2 Added value of the three-part bias correction

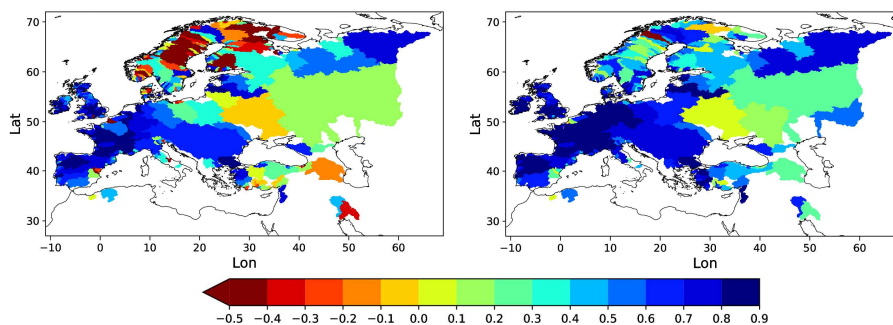
322 In this section, we consider the effect of the bias correction at the station locations and
 323 investigate whether the three-part bias correction adds value compared to using only the mean
 324 bias correction. For this purpose, we use HD5-WFDE5 and the period 1979-2014.

325 **Table 3.** Mean bias and KGE of simulated (HD5-WFDE5) and bias corrected discharge
 326 for selected rivers during 1979-2014.

River	HD5-WFDE5		Mean Bias corr.		3-part Bias corr.	
	Bias	KGE	Bias	KGE	Bias	KGE
Dalaelven	-32.02 %	-0.32	0 %	-0.28	0.01 %	0.48
Elbe	36.44 %	0.46	0 %	0.60	-0.06 %	0.85
Indalsaelven	-19.32 %	-0.79	0 %	-0.78	-0.02 %	0.38
Odra	41.30 %	0.14	0 %	0.25	0.01 %	0.75
Rhine	14.60 %	0.74	0 %	0.78	-0.02 %	0.85
Weser	33.15 %	0.55	0 %	0.70	-0.01 %	0.90

327

328



329

330

331 **Figure 6.** Kling Gupta efficiencies for bias corrected HD5-WFDE5 discharges using the
 332 mean bias correction (left) and the three-part bias correction (right) during 1979-2014.

333 Both bias correction methods reduce the mean discharge bias to zero or close to zero in the
 334 case of the three-part bias correction due to the smoothing around the percentile range
 335 thresholds (see Table 3 for selected rivers). When the mean bias correction is applied, the KGEs
 336 (Figure 6 – left panel) are noticeably improved over Western and Central Europe. However,
 337 with a few exceptions, the KGE pattern over Northern Europe and other areas remains largely
 338 unchanged. This indicates that a correction of the long-term bias in the annual mean discharge
 339 over these areas is not sufficient. Only with the three-part bias correction does the KGE (Figure



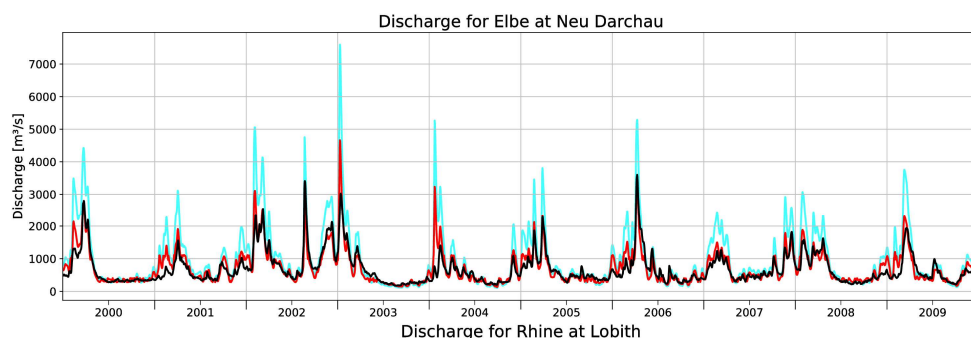
340 6 – right panel, Table 3 for selected rivers) improve considerably over these areas, with the
341 largest improvements occurring over Scandinavia. The three-part bias correction also leads to
342 some further improvements over Western and Central Europe, where the bias corrected
343 discharge with the mean bias correction already shows relatively high KGE values, e.g. for the
344 rivers Elbe, Rhine and Weser.

345 To visualise the effect of the three-part bias correction on the simulated daily discharges, we
346 consider the corresponding discharge curves for the period 2000-2009 for selected large rivers.
347 The respective biases and KGE are shown in Table 3 for the period 1979-2014. For the rivers,
348 Elbe, Weser and Oder, the peak discharges are generally overestimated, while the low flows
349 are close to the observed values (Figure 7). The correction of the high percentiles leads to a
350 considerable improvement in the representation of the peak discharges, while the change in the
351 low flows is rather small. The discharge of the Rhine (Figure 7) is well represented by HD5-
352 WFDE5. However, the small downward correction of the peak discharges and the slight
353 increase in the low flows still lead to an improved discharge curve, which is also indicated by
354 the increased KGE (Table 3).

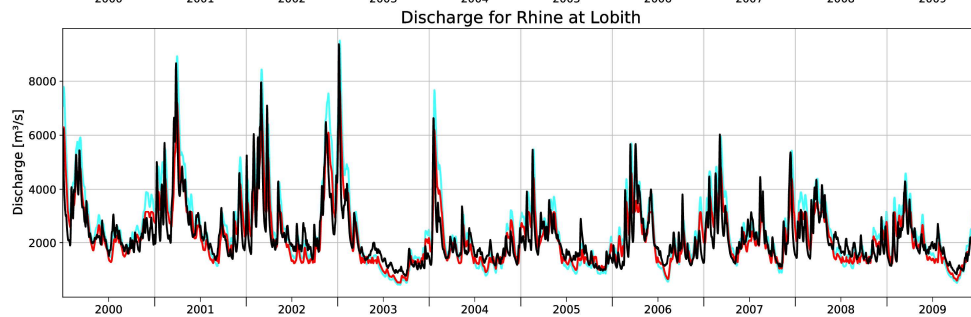
355 As mentioned above, the greatest improvements from the three-part bias correction
356 compared to the application of the mean bias correction occur over Scandinavia. Here many
357 rivers are highly regulated. For this reason, the discharge curves of the Daleaelven and
358 Indalsaelven rivers are examined in more detail in Figure 8. The observed discharges clearly
359 show the effect of the human regulation, where regulation leads to the elimination of peak
360 discharges, while maintaining certain flows during low flow periods. Figure 8 shows that, on
361 the one hand, peak discharges are often suppressed or reduced, especially during the spring,
362 and that, on the other hand, low-flow periods are either almost absent (especially for the
363 Indalsaelven) or show a rather noisy, unnatural daily variability. Here, the bias correction
364 partially mimics these regulation effects by reducing the peak discharges and increasing the low
365 flows.



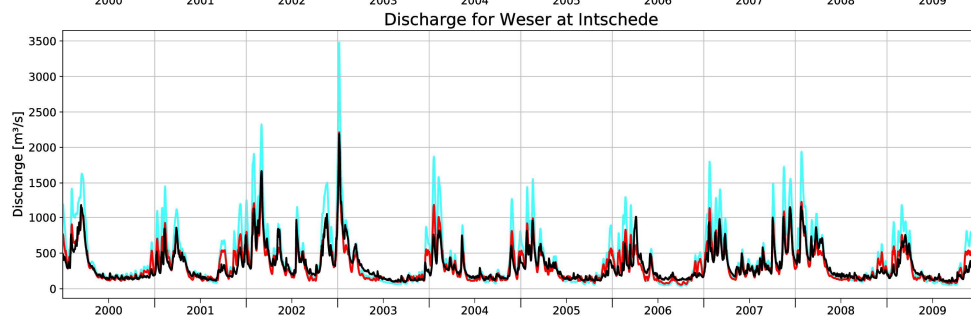
366



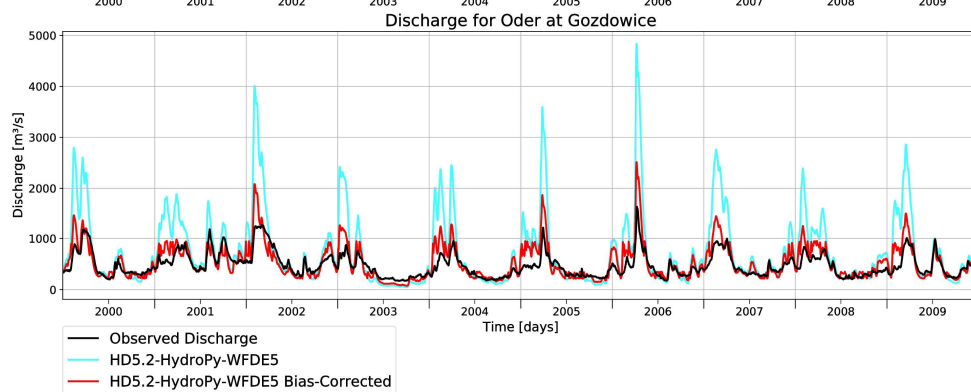
367



368



369



370

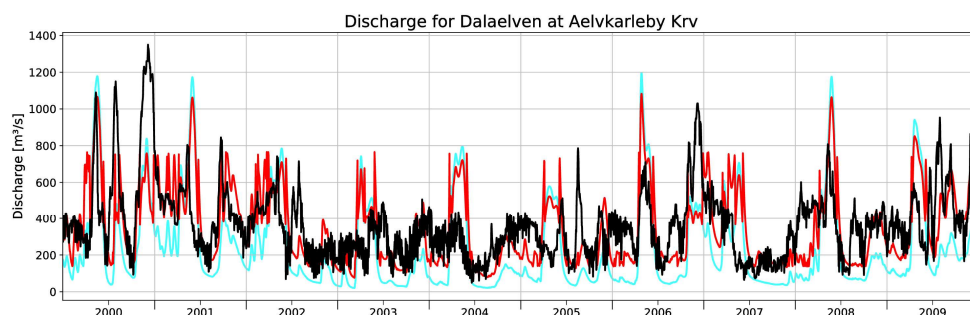
371

Figure 7. Observed and simulated daily discharges for the rivers Elbe (1st panel), Rhine (2nd panel), Weser (3rd panel) and Odra (4th panel) during 2000-2009.

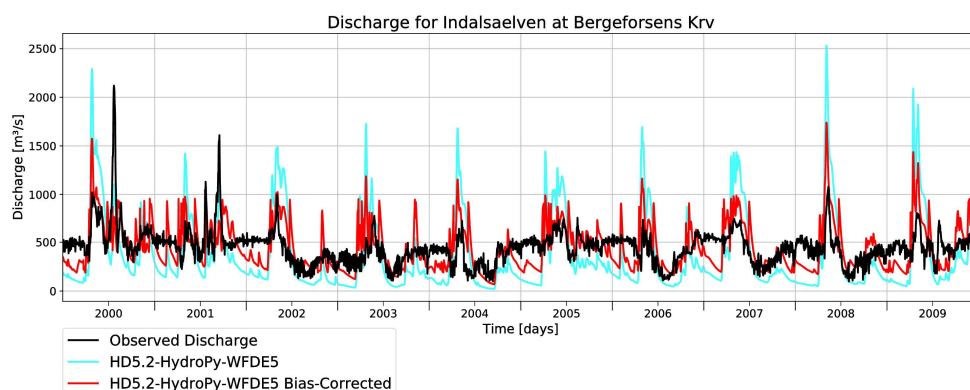
372



373



374



375

Figure 8. Observed and simulated daily discharges for the rivers Dalaelven (1st panel) and Indalsaelven (2nd panel) during 2000-2009.

376

377 3.3 Application of the bias correction for a different time period

378

To consider the effect of the bias correction for the applications over different time periods, we derived bias correction factors for HD5-GSWP3 during 1979-2014 and applied the factors for the period 1950-1978.

379

380

381

For HD5-GSWP3, the distributions of bias and Kling-Gupta efficiencies are quite similar between the two periods 1950-1978 (Figure 9 – left column) and 1979-2014 (Figure 5 – left column). Consequently, the bias correction leads to similar improvements in the KGE (Figure 9) as for the most recent period (not shown). The bias also becomes small for most of the rivers. Noticeable exceptions are the Dnjepr, Volga and some rivers in Southern Europe. This may be related to differences in the anthropogenic influence on the discharge between the two periods, as is the case for the river Ebro. Here, the large wet bias (51.65 %) in the more recent period is contrasted with a small wet bias (12.05%) in the earlier period (Figure 10). Since large anthropogenic water abstractions occur in the Ebro River (Merchán et al., 2013), this seems to be related to the different irrigation activities in the two periods, which are much more pronounced in the more recent years. The latter can be seen by looking at the observed daily discharges between 1960-1969 and 2000-2009 (Figure 10). In the earlier period, the Ebro discharge still shows some variations according to the sequence of weather events in the dry season. However, in the later period, the observed discharge includes only very small variations during the dry season, indicating more intense human water abstraction than in the earlier

392

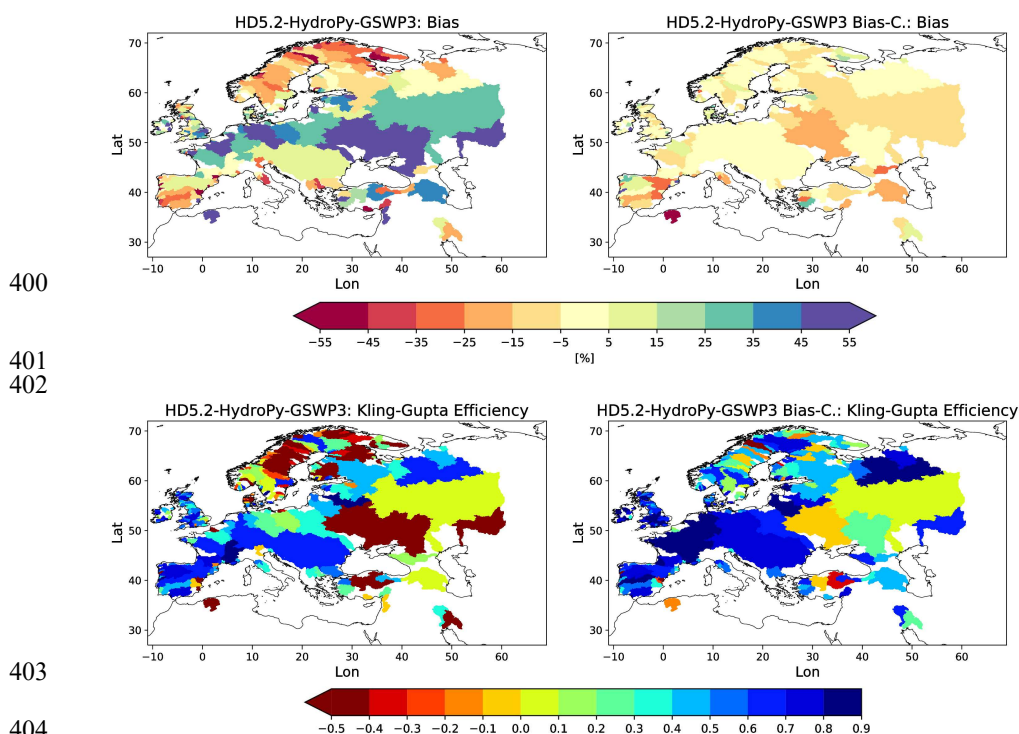
393

394

395



396 period. Consequently, the bias correction based on the recent wet bias leads to a dry bias (-
 397 25.78 %) in the corrected Ebro discharge in the earlier period. However, the KGE decreases
 398 only slightly from 0.68 to 0.63, so that the deterioration of the mean bias seems to be largely
 399 compensated by the correction of the different percentile ranges.



400

401
402

403

404

405 **Figure 9.** Mean discharge bias [%] (upper row) and Kling Gupta efficiencies (lower row)
 406 for HD5-GSWP3 (left) and bias corrected HD5-GSWP3 data (right) during 1950-
 407 1978.

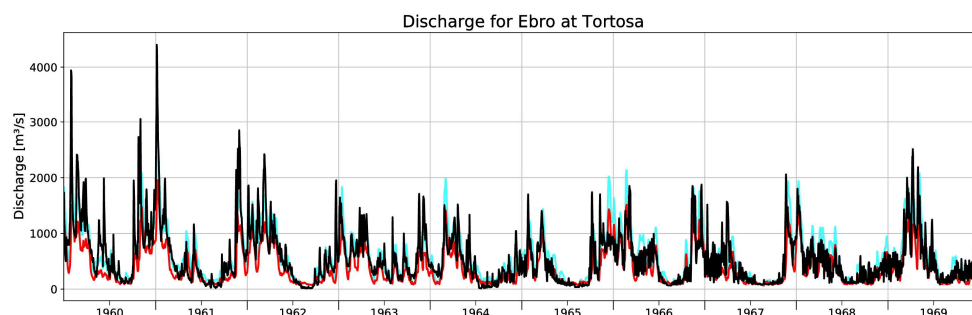
408 **4 Evaluation of the inflow into sea basins**

409 To evaluate the simulated and bias corrected discharges at the river mouths, we considered the
 410 integrated inflow into different sea basins. First, we evaluated the discharges into the Baltic Sea
 411 using HELCOM and IGC-EMO data in Section 4.1. We then compared the discharges to the
 412 North Sea and the Northeast Atlantic with OSPAR and up-scaled (see Section 2.5) IGC-EMO
 413 data in Section 4.2.

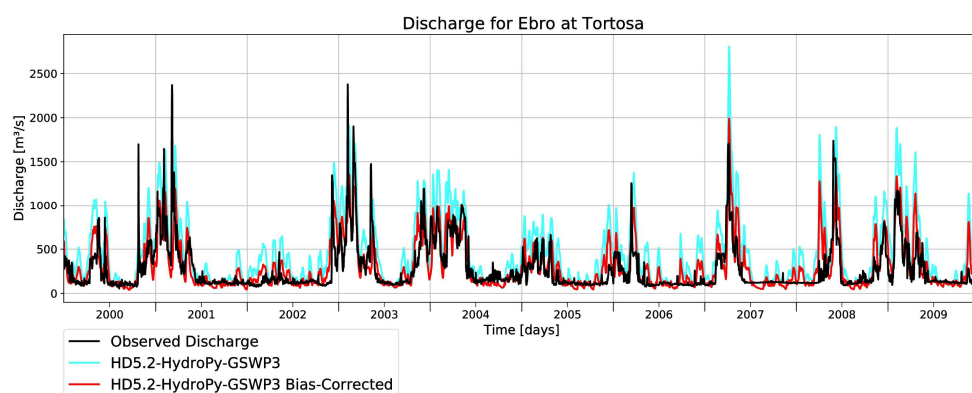
414



415



416



417

Figure 10. Observed and simulated daily discharge of HD5-GSWP3 for the Ebro river during 1960-1969 (1st panel) and 2000-2009 (2nd panel).

418

419

4.1 Baltic Sea

420

In order to achieve a maximum overlap of the simulated discharge time series data with the HELCOM data (cf. Section 2.5), we considered 1995-2019 as the evaluation period for the Baltic Sea and its seven sub-basins (Figure 4 – upper panel). For the whole Baltic Sea and most of its sub-basins, the bias correction improves the basin inflows if compared to the HELCOM estimates (Table 4, Figure 11). Only for the Gulf of Finland and the Gulf of Riga, the bias correction leads to a slightly larger bias while the biases of HD5-WFDE5 in these basins are relatively small. When the simulated inflows are compared with the IGC-EMO estimates, similar results are obtained, except for the Gulf of Riga. Here, the IGC-EMO estimates are about 32% larger than the HELCOM estimates, indicating a larger uncertainty in at least one of these two estimates. For the Gulf of Riga basin, the major part of the inflow is contributed by the Daugava river. In IGC-EMO, the discharge from the Daugava is based on observed time series from 1970-1990. These data were extended to earlier and later periods, e.g. by climatological values and trend preservation (Van Leeuwen and Hagemann, 2023). For 1970-1990, the mean IGC-EMO discharge comprises 623 m³/s at the Daugava mouth, while this has increased by ca. 45% in 1995-2019 (902 m³/s). However, this strong increase cannot be seen in the observed discharge time series at the station Daugavpils that covers about three quarter of the Daugava catchment. Here, the discharge increases only slightly from 1970-1999 (439 m³/s; 95% temporal data coverage) to 1995-2019 (452 m³/s; 83% temporal data coverage). This

437

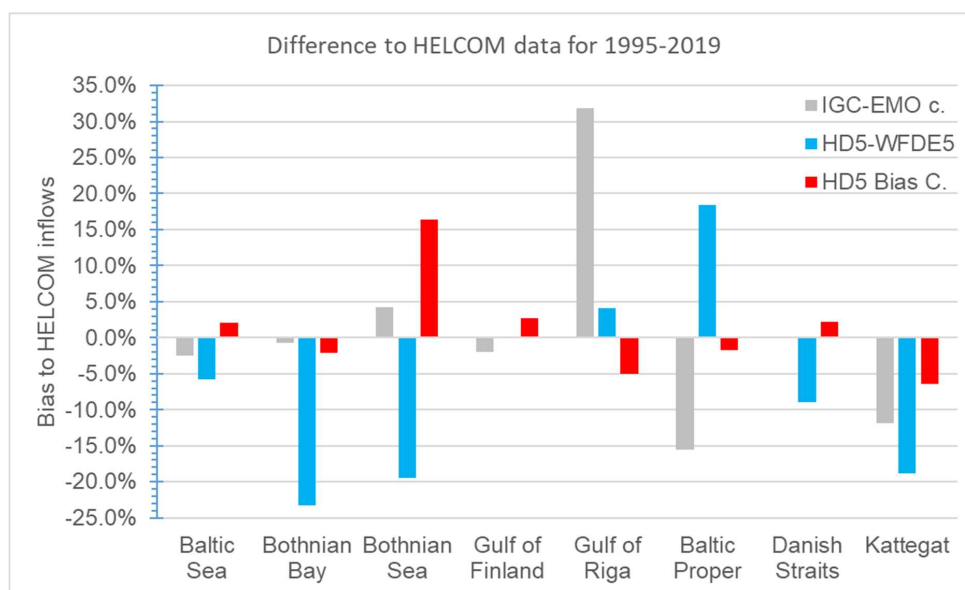


438 indicates a large overestimation of the IGC-EMO Daugava discharge during 1995-2019 and,
 439 hence, also of the respective Gulf of Riga inflow.

440 **Table 4.** Estimated and simulated inflows (unit: m³/s) into the Baltic Sea and its major
 441 sub-basins during 1995-2019. Note that for the Danish Straits no IGC-EMO estimate
 442 is provided as the respective catchment area coverage of the rivers in IGC-EMO is too
 443 low.

Sea basin	HELCOM	IGC-EMO c.	HD5-WFDE5	HD5 Bias C.
Baltic Sea	15676	15286	14764	15995
Bothnian Bay	3444	3420	2642	3369
Bothnian Sea	2913	3038	2347	3391
Gulf of Finland	3519	3448	3520	3612
Gulf of Riga	1071	1411	1114	1017
Baltic Proper	3436	2901	4070	3377
Danish Straits	217	0	198	222
Kattegat	1077	949	873	1008

444



445

446 **Figure 11.** Relative difference in basin inflows compared to HELCOM data for 1995-
 447 2019. Note that no IGC-EMO estimate is provided for the Danish Straits as the
 448 respective river catchment coverage in IGC-EMO is too small.

449 4.2 North Sea and Northeast Atlantic

450 Due to the different treatment of unmonitored regions by the OSPAR countries (cf. Section
 451 2.5), and thus of the respective sea basin areas, we have not corrected the OSPAR inflows.
 452 Instead, we have also considered up-scaled IGC-EMO data as alternative estimates of basin



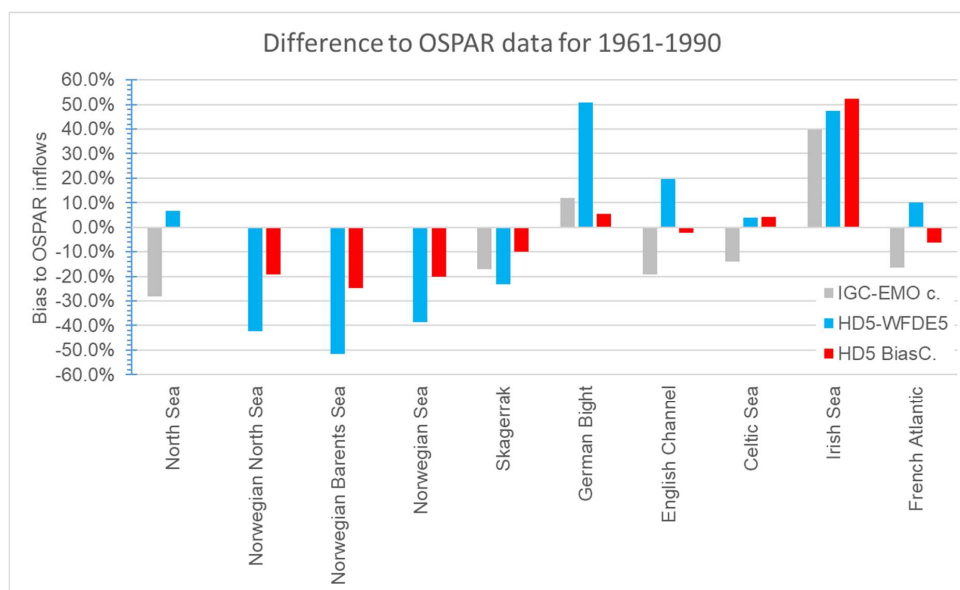
453 inflow (as in Section 4.1). Table 5 shows simulated and estimated basin inflows for the
 454 considered OSPAR regions (cf. Figure 4 – lower panel). Note that IGC-EMO data for the
 455 Norwegian shares of the Barents Sea, Norwegian Sea and North Sea, and the North Spanish
 456 Atlantic are not included in the following comparisons due to their limited area coverage. When
 457 comparing the simulated sea basin inflows with the OSPAR and IGC-EMO data, we found that
 458 the bias correction improves the simulated inflows for most of the OSPAR regions (Figure 12).
 459 Exceptions are the values for the Celtic Sea and the Irish Sea. For the Celtic Sea, the bias
 460 corrected inflows are very close to the uncorrected inflows and the difference to the OSPAR
 461 data is rather small. For the Irish Sea, the bias corrected inflows are somewhat larger than the
 462 uncorrected ones, with both showing large differences (52.5% and 47.5%) to the OSPAR data.
 463 Here both inflows are closer to the IGC-EMO estimate, which exceeds the OSPAR estimate by
 464 about 40%.

465 **Table 5.** Estimated and simulated inflows (unit: m³/s) into major sub-basins of the North
 466 Sea and the Northwest Atlantic during 1961-1990. Note that the North Sea does not
 467 comprise Skagerrak and the English Channel. Up-scaled IGC-EMO basin estimates
 468 for which the fractional area coverage of IGC-EMO rivers is less than 75% are
 469 considered as highly uncertain and are therefore only given in brackets (cf. Sect. 2.5).
 470 The same applies to the OSPAR inflow into the Northern Spanish Atlantic.

Sea basin	OSPAR	IGC-EMO c.	HD5-	
			WFDE5	HD5 BiasC.
North Sea	9190	6600	9798	9164
Norwegian North Sea	3534	(1499)	2038	2856
Norwegian Barents Sea	2294	-	1106	1723
Norwegian Sea	3663	-	2242	2922
Skagerrak	2544	2113	1956	2292
German Bight	1344	1505	2025	1419
English Channel	1250	1011	1498	1222
Celtic Sea	976	839	1016	1016
Irish Sea	672	939	992	1025
French Atlantic	2862	2391	3147	2684
Northern Spanish Atlantic	(359)	(1655)	1104	1550

471

472 While the OSPAR values from Ireland include estimates for unmonitored areas, this is not
 473 the case for the UK (Table 2). Farkas and Skarbøvik (2021) list the rivers contributing to the
 474 OSPAR value (560 m³/s) from the UK part of the Irish Sea catchment (35000 km²). Adding up
 475 the catchment areas of each river, obtained from various online resources, gives a coverage of
 476 about 70%. In order to account for this under-representation of the catchment area, an up-
 477 scaling can be performed, similar to the treatment of the IGC-EMO data. This would give an
 478 estimate of about 803 m³/s for the UK Irish Sea inflow and thus 915 m³/s for the whole Irish
 479 Sea. The respective IGC-EMO inflow is close to this value (+2.6%) and the overestimation of
 480 inflows is less pronounced for HD-WFDE5 and bias corrected discharges with +8.4% and
 481 +12% respectively.



482

483 **Figure 12.** Relative difference in basin inflows compared to OSPAR data for 1961-1990.
 484 IGC-EMO basin estimates for which the fractional area coverage is less than 75% are
 485 not shown.

486 4.3 Simulated salinity in the German Bight

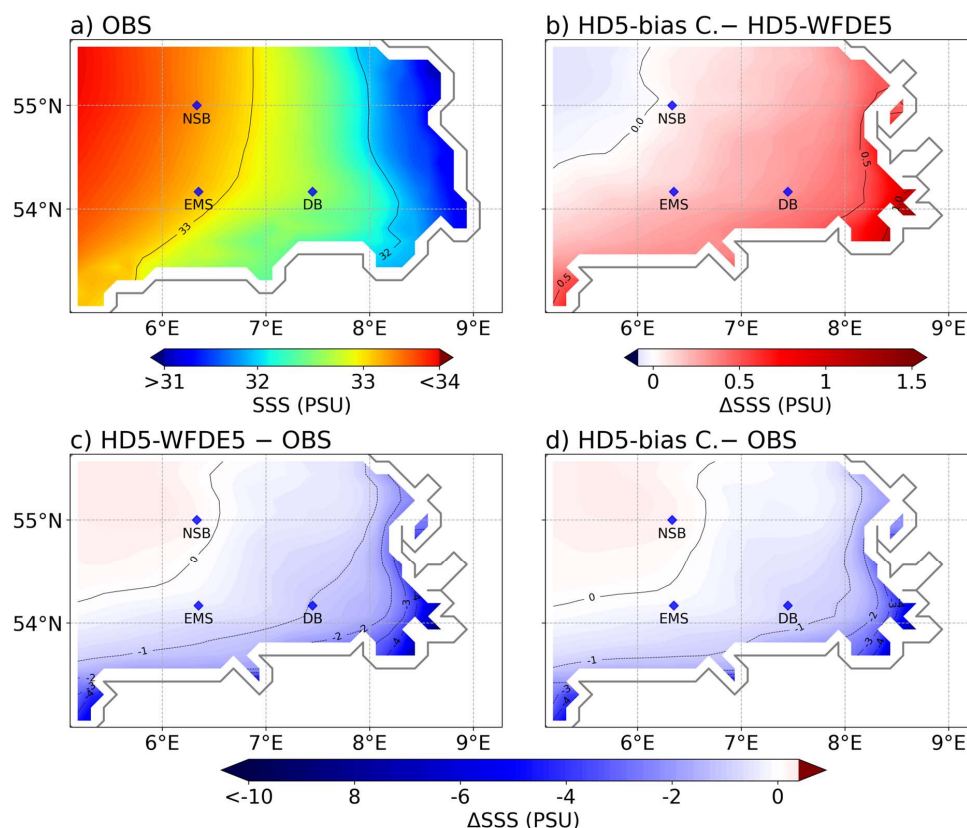
487 Using the two experiments described in Sect. 2.6, we evaluated the simulated sea surface
 488 salinity (SSS) with satellite-based analyses and in-situ observations for the period 2010 to 2018.
 489 The SSS analyses were derived using a multivariate optimal interpolation algorithm that
 490 combines sea surface salinity images from several satellite sources, such as the National
 491 Aeronautics and Space Administration (NASA) Soil Moisture Active Passive (SMAP) satellite
 492 and the European Space Agency (ESA) Soil Moisture Ocean Salinity (SMOS) satellite, with
 493 in-situ salinity measurements (Droghei et al., 2018). These SSS data are available with a spatial
 494 resolution of 0.125°.

495 Figure 13a shows the mean analysed SSS in the German Bight for the period 2010-2018,
 496 with lower salinities near the west coast of Germany and higher salinities towards the west. The
 497 NEMO simulation using the uncorrected discharges of HD5-WFDE5 (Figure 13c) has too low
 498 SSS in coastal areas, especially near the estuaries. This low bias is reduced using the bias
 499 corrected discharges (Figure 13d), as the general effect of the bias correction in the German
 500 Bight leads to reduced riverine inflows (cf. Figure 12) and hence increased SSS in coastal areas
 501 (Figure 13b).

502 In addition, we had access to salinity measurements at three stations in the German Bight
 503 operated by the BSH as part of the Marine Environmental Monitoring Network in the North
 504 and Baltic Seas (MARNET). These three stations are Deutsche Bucht (DB; located at 54.17°N,
 505 7.45°E), EMS (54.17°N, 6.35°E) and Nordsee Boje II (NSB; 55°N, 6.33°E) and their locations
 506 are shown in Figure 13. In general, the bias corrected discharges lead to an improved simulation
 507 of the daily salinity at 6 m depth at the stations DB and EMS. Here the RSME decreases from



508 1.70 to 1.45 and from 1.43 to 1.32, respectively. It seems that in NEMO the positive effect of
509 using bias corrected discharges is limited to near-surface salinities, as there is no noticeable
510 effect at 30 m depth (not shown). NSB is not considered in detail as it is located further offshore
511 where no noticeable SSS changes were introduced by using bias corrected discharges (Figure
512 13b).



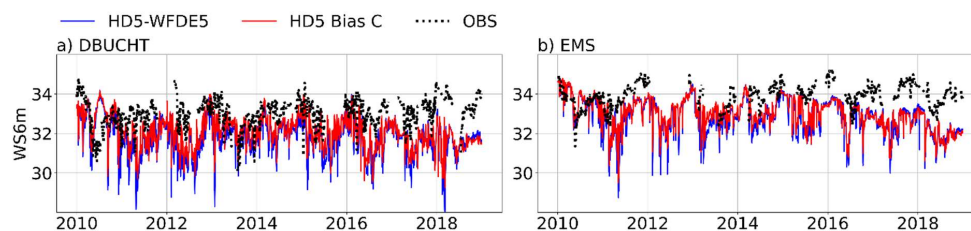
513

514 **Figure 13.** Mean analyzed SSS: a) OBS and various SSS differences of the NEMO
515 experiments in the German Bight for the period from 2010 to 2018. The SSS
516 differences comprise b) HD5-Bias C. minus HD5-WFDE5, c) HD5-WFDE5 minus
517 OBS, and d) HD5-Bias C. minus OBS.

518 In summary, the results of the NEMO experiments indicate the beneficial effect of using bias
519 corrected discharges on the simulated SSS in coastal areas. However, although the low SSS
520 biases are reduced by using the bias corrected discharges, the simulated SSS is still
521 underestimated in coastal areas, especially close to the estuaries of large rivers (Figure 13d).
522 This may be attributed to the rather smooth coastline of the NEMO ocean grid. Here, a major part
523 of the large estuaries of the rivers Elbe, Ems and Weser are not included. In reality, a major part
524 of the mixing of the riverine freshwater inflow and the saline North Sea happens within these
525 estuaries. In the NEMO model setup, the freshwater inflow is introduced at the respective river
526 mouth points of the smooth NEMO coastline where it starts to mix with the saline North Sea
527 water. Consequently, the simulated water at and near those points is much fresher than in reality,



528 which leads to the low SSS bias. Note that on the one hand such a smooth coastline is necessary
 529 in NEMO to avoid numerical instabilities. On the other hand, the spatial resolution of the
 530 NEMO grid is not high enough to adequately resolve parts of the longer estuaries.



531

532 **Figure 14.** Observed and simulated daily time series of salinity in 6 m depth for the
 533 MARNET stations: a) DB and b) EMS. Unit: PSU

534 5 Summary and Conclusions

535 In the present study, we have introduced a methodology for the bias correction of European
 536 river runoff to provide corrected riverine inflows as forcing for ocean models in offline and
 537 coupled system model simulations. The central part of this methodology is a three-part bias
 538 correction, which can correct different biases for low, medium and high discharges. The bias
 539 correction parameters are derived in two steps. First, different correction factors for low,
 540 medium and high flows are derived for each river considered (cf. Sect. 2.5) at the location of
 541 the most downstream station for which daily discharge measurements were available. These
 542 factors were then transferred to the respective river mouth on the HD model grid and to adjacent
 543 coastal inflow points in its vicinity.

544 The evaluation of the bias corrected discharge at the station location showed that the bias
 545 correction greatly improved the simulated discharges. For the evaluation of the bias corrected
 546 discharge at the downstream station locations, we considered the mean bias and the KGE, which
 547 is a quality metric combining bias, correlation and coefficient of variation. Considering the
 548 same period as used to derive the bias correction factors, the mean bias is trivially close to zero.
 549 However, the bias is also substantially reduced for most rivers if a different period is considered.
 550 Irrespective of the period, the KGE pattern generally improves for the bias corrected discharges
 551 and shows high values for many rivers. Exceptions are those rivers with a very strong
 552 anthropogenic distortion of the natural flow, e.g. by many dams or large water withdrawals.
 553 Here, despite of some improvements, the KGE values are still rather low, such as for the rivers
 554 Dnjepr, Volga, Luleälven and a few Turkish rivers flowing into the Black Sea. The KGE also
 555 shows the beneficial effect of the three-part bias correction, as correcting only the long-term
 556 mean annual discharge bias is not sufficient in many areas, especially in northern Europe. We
 557 found that the three-part bias correction often improves the KGE in regulated rivers, so that it
 558 appears to mimic the effect of regulation, where regulation leads to the elimination of peak
 559 flows while maintaining certain flow levels during low flow periods.

560 The evaluation of riverine inflows to the sea at river mouths with observed daily discharge
 561 is rarely possible as there are usually no river gauges available. Even if there is a gauge at the
 562 mouth of a river, the measurements are often affected by tidal influences from the coast, so that
 563 the measured amounts may not represent the actual river discharge. For obvious reasons, it is
 564 also difficult to compare simulated inflows with observed discharges for unmonitored rivers.



565 Therefore, we compared the simulated and bias corrected discharges with long-term mean
566 inflow estimates into different sea basins from HELCOM, OSPAR and IGC-EMO. For most of
567 the basins considered, the bias correction improves the simulated inflows. This indicates a
568 reasonable performance of the approach to transfer the bias correction factors obtained at the
569 downstream stations to the respective river mouths and adjacent coastal areas. Exceptions are
570 the Gulf of Finland, the Gulf of Riga, the Celtic Sea and the Irish Sea. For the Gulf of Finland
571 and the Celtic Sea, the deviations of the uncorrected and bias corrected inflows from the inflow
572 estimates are rather small. For the Gulf of Riga, the deviations of the uncorrected and bias
573 corrected inflows from the HELCOM estimates are also small, but they significantly
574 underestimate the IGC-EMO estimates. However, this could be due to a large overestimation
575 of the Daugava discharge during the period 1995-2019 in the IGC-EMO data and thus also of
576 the corresponding Gulf of Riga inflow. For the Irish Sea, IGC-EMO seems to be closer to reality
577 as the OSPAR inflow does not cover the unmonitored rivers in the British part of the catchment.

578 A caveat applies for rivers where the human influence on river flow has changed
579 significantly over time. Applying bias correction factors derived for 1979-2014 to earlier
580 periods may lead to errors for regulated rivers in years before these regulatory measures were
581 implemented. This is the case for the Ebro, where irrigation activities have largely intensified
582 during the period 1979-2014 compared to earlier periods (see Sect. 3.3). A detailed analysis of
583 the rivers and periods concerned is beyond the scope of this study. However, at least for the
584 period 1950-1978, the KGE distribution does not seem to be significantly affected, as there is
585 no noticeable deterioration.

586 We have shown that our bias correction method works well for Europe at the station
587 locations as well as for the riverine inflow into northern and western European sea basins. Using
588 two NEMO simulations in the German Bight, we have also shown that the use of the bias
589 corrected discharges as forcing leads to an improved simulation of sea surface salinity in coastal
590 areas. However, for the potential transfer of the bias correction methodology to other regions,
591 it has to be pointed out that the application of the three-part bias correction over a region only
592 makes sense if a large part of the catchment area is covered by available daily discharge
593 measurements. As the three-part bias correction is based on biases in three percentile ranges of
594 daily flows, it is also suitable for the use in climate change applications. Here the bias correction
595 factors can be derived from a historical discharge simulation and then applied to future
596 projections or past reconstructions. In addition, the bias correction can also be applied in
597 Regional Coupled System Model (RCSM) simulations, where the bias correction factors can
598 be derived from an initial simulation and then applied during the run-time of the actual RCSM
599 simulation. This capability has been implemented in the HD model v5.2.2 (Hagemann et al.,
600 2023b) and is currently being applied in the GCOAST AHOI system (Ho-Hagemann et al.,
601 2020). Finally, we note that the bias corrected discharges are available from the World Data
602 Centre for Climate and are already used within the CoastalFutures project
603 (<https://www.coastalfutures.de>).

604 **Data Availability Statement**

605 Many of the observed daily discharge data used can be obtained from the GRDC
606 (https://grdc.bafg.de/GRDC/EN/02_srvcs/21_tmsrs/riverdischarge_node.html). Other data
607 have been retrieved from public websites associated with the sources referred to in Sect. 2.5.
608 GSWP3 data were retrieved from the ISIMIP data portal (<https://data.isimip.org>) and WFDE5
609 data were retrieved from the Copernicus Climate Data Store (<https://cds.climate.copernicus.eu>).
610 OSPAR data were taken from an OSPAR report (Farkas and Skarbøvik, 2021) or its associated



611 data available on the OSPAR webpage ([https://odims.ospar.org/en/search/?dataset=rid-data-](https://odims.ospar.org/en/search/?dataset=rid-data-reports)
612 [reports](https://odims.ospar.org/en/search/?dataset=rid-data-reports)). This study has been conducted using E.U. Copernicus Marine Service Information
613 data on SSS (<https://doi.org/10.48670/moi-00051>) and some French discharge measurements.
614 The daily data of surface runoff and subsurface runoff as well as the simulated and bias
615 corrected discharge data (Hagemann and Stacke, 2023) can be accessed via the World Data
616 Centre for Climate (WDCC) at DKRZ.

617 **Acknowledgments**

618 This study was conducted within the CoastalFutures project that was funded by the German
619 Federal Ministry of Education and Research under grant number 03F0911E. TN was supported
620 by the subproject ‘A6 - The earth system variability and predictability in changing climate’ of
621 Germany’s Excellence Strategy EXC 2037 ‘CLICCS - Climate, Climatic Change, and Society’
622 with project no. 390683824, funded by the Deutsche Forschungsgemeinschaft (DFG, German
623 Research Foundation). We thank the DKRZ for providing the computing resources to perform
624 the HD simulations. We acknowledge the Copernicus Climate Data Store and the ISIMIP
625 project for making WFDE5 and GSWP3 datasets available. We are deeply indebted to all data
626 providers. We are also grateful to Sonja van Leuwen (Royal Netherlands Institute for Sea
627 Research) for providing us with the latest version of the IGC-EMO data. We are thankful to
628 Sebastian Grayek (Helmholtz-Zentrum Hereon) for the discussion on his NEMO results using
629 an initial version of the bias corrected discharges. Finally, we thank Tobias Stacke (Max Planck
630 Institute for Meteorology) for conducting the HydroPy simulations published in Hagemann and
631 Stacke (2023).

632 **Author Contributions**

633 SH developed and applied the three-part bias correction, conducted the discharge simulations
634 and analysis of results, and wrote the manuscript. HH conducted the NEMO simulations, helped
635 with the analysis of results and revised the manuscript. TN evaluated the SSS data of the NEMO
636 simulations, helped with the analysis of results and revised the manuscript.

637 **Conflict of Interest Statement**

638 The authors declare that the research was conducted in the absence of any commercial or
639 financial relationships that could be construed as a potential conflict of interest.

640 **References**

641

- 642 Becker, G. A., Dick, S., and Dippner, J. W.: Hydrography of the German Bight, *Mar. Ecol.*
643 *Prog. Ser.*, 91, 9-18, <https://doi.org/10.3354/meps091009>, 1992.
- 644 Borgvang, S. A., Skarbøvik, E., and Pengerud, A.: RID 2006 data report: Presentation and
645 Assessment of the OSPAR Contracting Parties’ RID 2006 Data., Norwegian Institute for
646 Agricultural and Environmental Research, London, No. 376/2008, 373 pp., 2008.
- 647 Budhathoki, A., Tanaka, T., and Tachikawa, Y.: Correcting streamflow bias considering its
648 spatial structure for impact assessment of climate change on floods using d4PDF in the
649 Chao Phraya River Basin, Thailand, *J. Hydrol.-Reg. Stud.*, 42,
650 <https://doi.org/10.1016/j.ejrh.2022.101150>, 2022.
- 651 Compo, G. P., Whitaker, J. S., Sardeshmukh, P. D., Matsui, N., Allan, R. J., Yin, X., Gleason,
652 B. E., Vose, R. S., Rutledge, G., Bessemoulin, P., Bronnimann, S., Brunet, M.,



- 653 Crouthamel, R. I., Grant, A. N., Groisman, P. Y., Jones, P. D., Kruk, M. C., Kruger, A. C.,
654 Marshall, G. J., Maugeri, M., Mok, H. Y., Nordli, O., Ross, T. F., Trigo, R. M., Wang, X.
655 L., Woodruff, S. D., and Worley, S. J.: The Twentieth Century Reanalysis Project, Q. J.
656 Roy. Meteor. Soc., 137, 1-28, <https://doi.org/10.1002/qj.776>, 2011.
- 657 Cucchi, M., Weedon, G. P., Amici, A., Bellouin, N., Lange, S., Schmied, H. M., Hersbach,
658 H., and Buontempo, C.: WFDE5: bias-adjusted ERA5 reanalysis data for impact studies,
659 Earth Syst. Sci. Data, 12, 2097–2120-2097–2120, [https://doi.org/10.5194/essd-12-2097-](https://doi.org/10.5194/essd-12-2097-2020)
660 [2020](https://doi.org/10.5194/essd-12-2097-2020), 2020.
- 661 Daewel, U., and Schrum, C.: Low-frequency variability in North Sea and Baltic Sea identified
662 through simulations with the 3-D coupled physical–biogeochemical model ECOSMO,
663 Earth Syst. Dyn., 8, 801-801, <https://doi.org/10.5194/esd-8-801-2017>, 2017.
- 664 Daraio, J. A.: Hydrologic Model Evaluation and Assessment of Projected Climate Change
665 Impacts Using Bias-Corrected Stream Flows, Water, 12,
666 <https://doi.org/10.3390/w12082312>, 2020.
- 667 Dirmeyer, P. A., Gao, X., Zhao, M., Guo, Z., Oki, T., and Hanasaki, N.: GSWP-2:
668 Multimodel Analysis and Implications for Our Perception of the Land Surface, Bull. Amer.
669 Meteor. Soc., 87, 1381-1398, <https://doi.org/10.1175/bams-87-10-1381>, 2006.
- 670 Droghei, R., Buongiorno Nardelli, B., and Santoleri, R.: A New Global Sea Surface Salinity
671 and Density Dataset From Multivariate Observations (1993–2016), Front. Mar. Sci., 5,
672 <https://doi.org/10.3389/fmars.2018.00084>, 2018.
- 673 Farkas, C., and Skarbøvik, E.: OSPAR Contracting Parties' RID 2019 Data Report, NIBIO –
674 Norwegian Institute for Bioeconomy Research, 57 pp., 2021.
- 675 Farmer, W. H., Over, T. M., and Kiang, J. E.: Bias correction of simulated historical daily
676 streamflow at ungauged locations by using independently estimated flow duration curves,
677 Hydrol. Earth Syst. Sci., 22, 5741-5758, <https://doi.org/10.5194/hess-22-5741-2018>, 2018.
- 678 Gupta, H. V., Kling, H., Yilmaz, K. K., and Martinez, G. F.: Decomposition of the mean
679 squared error and NSE performance criteria: Implications for improving hydrological
680 modelling, J. Hydrol., 377, 80–91-80–91, <https://doi.org/10.1016/j.jhydrol.2009.08.003>,
681 2009.
- 682 Hagemann, S., Stacke, T., and Ho-Hagemann, H. T. M.: High Resolution Discharge
683 Simulations Over Europe and the Baltic Sea Catchment, Front. Earth Sci., 8,
684 <https://doi.org/10.3389/feart.2020.00012>, 2020.
- 685 Hagemann, S., and Stacke, T.: Complementing ERA5 and E-OBS with high-resolution river
686 discharge over Europe, Oceanologia, 65, 230-248,
687 <https://doi.org/10.1016/j.oceano.2022.07.003>, 2022.
- 688 Hagemann, S., Ho-Hagemann, H. T. M., and Hanke, M.: The Hydrological Discharge Model -
689 a river runoff component for offline and coupled model applications. Zenodo.
690 <https://doi.org/10.5281/zenodo.7890682>, 2023.
- 691 Hagemann, S., and Stacke, T.: Bias corrected high resolution river runoff over Europe. World
692 Data Center for Climate (WDCC) at DKRZ.
693 https://doi.org/10.26050/WDCC/Biasc_hr_riverro_Eu, 2023.
- 694 HELCOM: The Third Baltic Sea Pollution Load Compilation, Balt. Sea Environ. Proc., no 70,
695 Baltic Marine Environment Protection Commission--Helsinki Commission, Helsinki,
696 Finland, 134 p. pp., 1998.
- 697 Hersbach, H., Bell, B., Berrisford, P., Hirahara, S., Horányi, A., Muñoz-Sabater, J. n.,
698 Nicolas, J., Peubey, C., Radu, R., Schepers, D., Simmons, A., Soci, C., Abdalla, S.,
699 Abellan, X., Balsamo, G., Bechtold, P., Biavati, G., Bidlot, J., Bonavita, M., Chiara, G.,
700 Dahlgren, P., Dee, D., Diamantakis, M., Dragani, R., Flemming, J., Forbes, R., Fuentes,
701 M., Geer, A., Haimberger, L., Healy, S., Hogan, R. J., Hólm, E. a., Janisková, M., Keeley,



- 702 S., Laloyaux, P., Lopez, P., Lupu, C., Radnoti, G., Rosnay, P., Rozum, I., Vamborg, F.,
703 Guillaume, S., and Thépaut, J.-N.: The ERA5 global reanalysis, *Quart. J. Roy. Meteor. Soc.*,
704 146, 1999-2049, <https://doi.org/10.1002/qj.3803>, 2020.
- 705 Ho-Hagemann, H. T. M., Hagemann, S., Grayek, S., Petrik, R., Rockel, B., Staneva, J., Feser,
706 F., and Schrum, C.: Internal Model Variability of the Regional Coupled System Model
707 GCOAST-AHOI, *Atmos.*, 11, 227-227, <https://doi.org/10.3390/atmos11030227>, 2020.
- 708 Hordoir, R., Polcher, J., Brun-Cottan, J. C., and Madec, G.: Towards a parametrization of
709 river discharges into ocean general circulation models: a closure through energy
710 conservation, *Clim. Dyn.*, 31, 891-908, <https://doi.org/10.1007/s00382-008-0416-4>, 2008.
- 711 Hordoir, R., and Meier, H. E. M.: Freshwater fluxes in the Baltic Sea: A model study, *J.*
712 *Geophys. Res.*, 115, C08028-C08028, <https://doi.org/10.1029/2009jc005604>, 2010.
- 713 ISIMIP2a Simulation protocol (extended version):
714 https://www.isimip.org/documents/647/ISIMIP2a_protocol_230302.pdf, access: 8.3.,
715 2023.
- 716 Kim, H.: Global Soil Wetness Project Phase 3 Atmospheric Boundary Conditions
717 (Experiment 1). Data Integration and Analysis System (DIAS).
718 <https://doi.org/10.20783/DIAS.501>, 2017.
- 719 Kim, K. B., Kwon, H. H., and Han, D. W.: Bias-correction schemes for calibrated flow in a
720 conceptual hydrological model, *Hydrol. Res.*, 52, 196-211,
721 <https://doi.org/10.2166/nh.2021.043>, 2021.
- 722 Kling, H., Fuchs, M., and Paulin, M.: Runoff conditions in the upper Danube basin under an
723 ensemble of climate change scenarios, *J. Hydrol.*, 424-425, 264-277-264-277,
724 <https://doi.org/10.1016/j.jhydrol.2012.01.011>, 2012.
- 725 Knoben, W. J. M., Freer, J. E., and Woods, R. A.: Technical note: Inherent benchmark or not?
726 Comparing Nash-Sutcliffe and Kling-Gupta efficiency scores, *Hydrol. Earth Syst. Sci.*, 23,
727 4323-4331, <https://doi.org/10.5194/hess-23-4323-2019>, 2019.
- 728 Lehmann, A., and Hinrichsen, H.-H.: On the thermohaline variability of the Baltic Sea, *J.*
729 *Mar. Syst.*, 25, 333-357, [https://doi.org/10.1016/s0924-7963\(00\)00026-9](https://doi.org/10.1016/s0924-7963(00)00026-9), 2000.
- 730 Lenhart, H. J., Mills, D. K., Baretta-Bekker, H., van Leeuwen, S. M., van der Molen, J.,
731 Baretta, J. W., Blaas, M., Desmit, X., Kuhn, W., Lacroix, G., Los, H. J., Menesguen, A.,
732 Neves, R., Proctor, R., Ruardij, P., Skogen, M. D., Vanhoutte-Brunier, A., Villars, M. T.,
733 and Wakelin, S. L.: Predicting the consequences of nutrient reduction on the eutrophication
734 status of the North Sea, *J. Mar. Syst.*, 81, 148-170,
735 <https://doi.org/10.1016/j.jmarsys.2009.12.014>, 2010.
- 736 Madadgar, S., Moradkhani, H., and Garen, D.: Towards improved post-processing of
737 hydrologic forecast ensembles, *Hydrol. Process.*, 28, 104-122,
738 <https://doi.org/10.1002/hyp.9562>, 2014.
- 739 Madec, G., Bourdallé-Badie, R., Bouttier, P.-A., Bricaud, C., Bruciaferr, D., Calvert, D.,
740 Chanut, J., Clementi, E., Coward, A., Delrosso, D., Ethé, C., Flavoni, S., Graham, T.,
741 Harle, J., Iovino, D., Lea, D., Lévy, C., Lovato, T., Martin, N., and Vancoppenolle, M.:
742 NEMO ocean engine. Notes du Pôle de modélisation de l'Institut Pierre-Simon Laplace
743 (IPSL), 27, Zenodo, <https://doi.org/10.5281/zenodo.3248739>, 2017.
- 744 Malek, K., Reed, P., Zeff, H., Hamilton, A., Wrzesien, M., Holtzman, N., Steinschneider, S.,
745 Herman, J., and Pavelsky, T.: Bias correction of hydrologic projections strongly impacts
746 inferred climate vulnerabilities in institutionally complex water systems, *J. Water Res.*
747 *Plan. Man.*, 148, [https://doi.org/10.1061/\(Asce\)Wr.1943-5452.0001493](https://doi.org/10.1061/(Asce)Wr.1943-5452.0001493), 2022.
- 748 Marzeion, B., Levermann, A., and Mignot, J.: The Role of Stratification-Dependent Mixing
749 for the Stability of the Atlantic Overturning in a Global Climate Model*, *J. Phys.*
750 *Oceanogr.*, 37, 2672-2681-2672-2681, <https://doi.org/10.1175/2007jpo3641.1>, 2007.



- 751 Merchán, D., Causapé, J., and Abrahao, R.: Impact of irrigation implementation on hydrology
752 and water quality in a small agricultural basin in Spain, *Hydrol. Sci. J.*, 58, 1400–1413–
753 1400–1413, 2013.
- 754 Nguyen, T. T., Staneva, J., Grayek, S., Bonaduce, A., Hagemann, S., Pham, N. T., Kumar, R.,
755 and Rakovec, O.: Impacts of extreme river discharge on coastal dynamics and
756 environment: Insights from high-resolution modeling in the German Bight, *Reg. Stud.*
757 *Mar. Sci.*, 73, <https://doi.org/10.1016/j.rsma.2024.103476>, 2024.
- 758 Shi, X. G., Wood, A. W., and Lettenmaier, D. P.: How Essential is Hydrologic Model
759 Calibration to Seasonal Streamflow Forecasting?, *J. Hydrometeorol.*, 9, 1350–1363,
760 <https://doi.org/10.1175/2008jhm1001.1>, 2008.
- 761 Stacke, T., and Hagemann, S.: HydroPy (v1.0): A new global hydrology model written in
762 Python, *Geosci. Model Dev.*, <https://doi.org/10.5194/gmd-2021-53>, 2021.
- 763 Väli, G., Meier, H. E. M., and Elken, J.: Simulated halocline variability in the Baltic Sea and
764 its impact on hypoxia during 1961–2007, *J. Geophys. Res. Oceans*, 118, 6982–7000–6982–
765 7000, <https://doi.org/10.1002/2013jc009192>, 2013.
- 766 Van Leeuwen, S., and Lenhart, H. J.: OSPAR ICG-EMO riverine database 2020-05-01 used
767 in 2020 workshop. NIOZ, V1. <https://doi.org/10.25850/nioz/7b.b.vc>, 2021.
- 768 Van Leeuwen, S., and Hagemann, S.: Mapping of IGC-EMO nutrient loads on the high
769 resolution HD model grid (Version 1). World Data Center for Climate (WDCC) at DKRZ.
770 https://doi.org/10.26050/WDCC/IGC-EMO_HD_v1, 2023.
- 771 Warszawski, L., Frieler, K., Huber, V., Piontek, F., Serdeczny, O., and Schewe, J.: The Inter-
772 Sectoral Impact Model Intercomparison Project (ISI-MIP): Project framework, *Proc. Natl.*
773 *Acad. Sci. USA*, 111, 3228–3232, <https://doi.org/10.1073/pnas.1312330110>, 2014.
- 774 Weedon, G. P., Gomes, S., Viterbo, P., Shuttleworth, W. J., Blyth, E., Österle, H., Adam, J.
775 C., Bellouin, N., Boucher, O., and Best, M.: Creation of the WATCH Forcing Data and Its
776 Use to Assess Global and Regional Reference Crop Evaporation over Land during the
777 Twentieth Century, *J. Hydrometeorol.*, 12, 823–848,
778 <https://doi.org/10.1175/2011JHM1369.1>, 2011.
- 779 Yoshimura, K., and Kanamitsu, M.: Dynamical global downscaling of global reanalysis, *Mon.*
780 *Weather Rev.*, 136, 2983–2998, <https://doi.org/10.1175/2008mwr2281.1>, 2008.
- 781 Zuo, H., Balmaseda, M. A., Tietsche, S., Mogensen, K., and Mayer, M.: The ECMWF
782 operational ensemble reanalysis–analysis system for ocean and sea ice: a description of the
783 system and assessment, *Ocean Sci.*, 15, 779–808, <https://doi.org/10.5194/os-15-779-2019>,
784 2019.

785